

Adhesive-free bonded crystalline Yb:YAG for high energy laser applications

Contact mariastefania.de-vido@stfc.ac.uk

Mariastefania De Vido, Klaus Ertel, Jonathan Phillips, Paul Mason, Saumyabrata Banerjee, Thomas Butcher, Jodie Smith, Chris Edwards, Cristina Hernandez-Gomez, John Collier

Central Laser Facility, STFC Rutherford Appleton Laboratory, Didcot, OX11 0QX, UK;

Abstract

We report on the application of the adhesive-free bonding (AFB) technique to form Yb-doped crystalline Yttrium Aluminum Garnet (Yb:YAG) gain media slabs. We performed experiments to characterise mechanical strength, optical quality and laser-induced damage threshold (LIDT) of bonded substrates. We demonstrate that mechanical properties of bonded samples are similar to those of monolithic substrates. We show that the presence of a bonding interface does not introduce unwanted wavefront deformations and does not increase the probability of laser-induced damage onset. Results indicate that the AFB technique constitutes a viable alternative for producing large aperture gain media slabs required for high-energy laser systems.

Introduction

Laser amplifiers capable of producing energetic nanosecond pulses are one of the main tools for ultra-high intensity laser-matter interaction research and high-energy applications such as particle acceleration [1, 2], intense X-ray generation [3], and inertial confinement fusion [4]. Proof-of-principle demonstrations have so far been performed using facilities relying on flash-lamp pumped systems, which are limited in terms of pulse repetition rates and efficiencies [5]. This leads to a limitation on the amount of science which can be carried out and prevents the translation of laser-plasma interactions into practical applications. An innovative approach, based on diode-pumped solid-state laser (DPSSL) technology allows overcoming these limitations as it enables multi-J pulse energy production at multi-Hz repetition rate operation [6-8]. Yb³⁺-doped Yttrium Aluminum Garnet (Yb:YAG) is one of the most promising materials for high-energy, high repetition rate DPSSL systems. Indeed, Yb³⁺ is an active laser ion which offers long fluorescence lifetimes, reasonable gain cross-sections, and low quantum defect, with efficient and reliable high power laser diodes available at its pump wavelength. YAG as the host medium offers good thermo-mechanical and thermo-optical properties. Large-sized, high optical quality gain media are a prerequisite for high-energy class laser facilities since such systems require amplification stages with apertures in excess of 10 cm to produce the required energies. However, production of large-sized, high optical quality crystalline Yb:YAG is challenging both in terms of costs and of manufacturing time, thus imposing a limit on the size of gain media slabs. In this work, we investigate adhesive-free bonding (AFB) of crystalline Yb:YAG as an alternative way of manufacturing large-sized gain media slabs from smaller starting components. We demonstrate that the AFB technique can be successfully used to manufacture crystalline Yb-doped YAG slabs characterised by good mechanical strength, optical quality and by adequate resilience to nanosecond laser irradiation. We show that AFB crystalline Yb:YAG performs the same way as equivalently prepared blank samples, therefore demonstrating the capability of meeting both the large dimensions and the optical quality requirements for high-energy laser systems. We show that the presence of a bonding interface does not increase

David Meissner, Stephanie Meissner

Onyx Optics, Inc., 6551 Sierra Lane, Dublin, CA 94568, USA

the probability of laser-induced damage for both uncoated and anti-reflective (AR) coated Yb:YAG substrates.

Materials and methods

Crystalline Yb:YAG substrate preparation

Substrates used for studying the optical properties consisted of 2 at-% doped crystalline Yb:YAG. A first set of samples, further referred to as monolithic samples, consisted of three 24 mm × 24 mm × 7 mm Yb:YAG substrates polished on both 24 mm × 24 mm faces to rms surface roughness values below 0.5 nm. A second set of samples, further referred to as bonded samples, consisted of three 24 mm × 24 mm × 7 mm pieces, each of them obtained by bonding two 12 mm × 24 mm × 7 mm substrates using the AFB technique (Fig. 1). The maximum doping gradient over the samples under study is expected to be 0.015 at-%. The AFB technique, already discussed in previous publication [9-11], was developed by Onyx Optics, Inc. (USA) and enables the joining, at relatively low temperatures, of crystalline or glass optical materials without the use of organic or inorganic bonding aids. The bonding process relies on the formation of non-localised, long-range induced dipole – induced dipole bonds due to London – van der Waals dispersion forces between two starting components brought in close contact. The attractive potential due to London – van der Waals dispersion forces becomes substantial only when atomic scale average separation between starting components is achieved, thus entailing strict requirements on surface flatness and smoothness. Therefore, surfaces to be bonded were polished to surface flatness and rms roughness allowing an average gap distance of a few Angstroms between the surfaces to be bonded. To assure compatibility between starting pieces, each piece was pre-selected from the same Yb:YAG boule and its refractive index was checked using interferometric techniques.

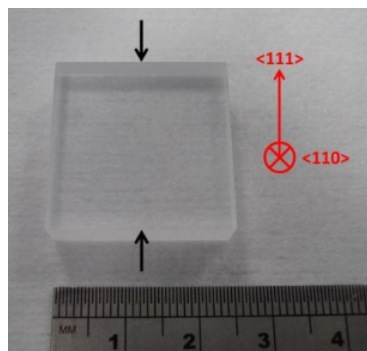


Fig. 1 Picture of a 24 mm x 24 mm x 7 mm bonded uncoated crystal Yb:YAG sample manufactured by Onyx Optics Inc. (USA). The black arrows indicate the position of the bonding interface. The red arrows indicate the crystal orientation.

Coating deposition

Gain media slabs for high-energy solid-state laser systems require AR coatings to reduce unwanted and potentially harmful reflections. Therefore, assessment of the performance of coatings deposited on bonded samples is critical to confirm the suitability of the AFB technique for high-energy laser systems. To this end, multilayer SiO₂/Ta₂O₅ AR coatings, designed for 99.75% transmission at both 939 nm and 1030 nm wavelengths,

were deposited on both monolithic and bonded substrates by Laseroptik GmbH (Germany). Two possible coating deposition techniques, widely applied to optical components for high energy laser systems, were used in this study, namely Ion Assisted Deposition (IAD) and Ion Beam Sputtering (IBS). Each coating technique was applied, during the same coating run, to both a monolithic and a bonded sample on one of the 24 mm × 24 mm polished surfaces.

Mechanical strength testing method

Gain media substrates can undergo stresses during processing and laser operation. Therefore, mechanical properties of bonded YAG samples were assessed for flexural strength at Onyx Optics, Inc. following the ASTM standard strength methods [12]. The Young's moduli (E) of both monolithic and bonded samples were measured using the setup depicted in Fig. 2(a), which was composed of a single column Instron load frame and a wavelength shifting interferometer VeriFire by Zygo mounted on a vibration isolated optical table. Each test sample underwent surface deformation due to an incrementally increasing load applied via a four point bending fixture, shown in Fig. 2(b).

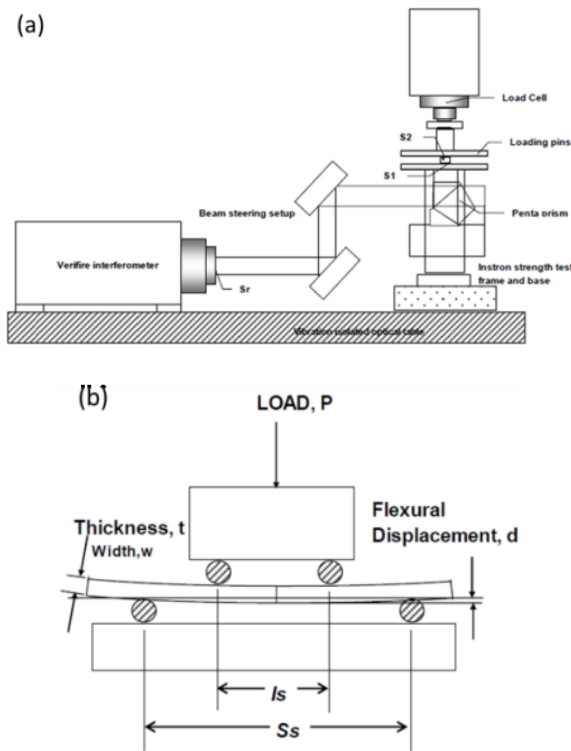


Fig. 2 Schematic drawing of the experimental setup used for the measurement of the Young's modulus of monolithic and bonded YAG samples (a) and of the four point bending test ($S_s = 40$ mm, $l_s = 20$ mm) (b).

Strength tests were carried out on tetragonal 3 mm × 4 mm × 50 mm substrates, as specified in the standard. Three configurations of AFB interface plane orientations, shown in Fig. 3, and further referred to as Type I, Type II and Type III, were taken into account.

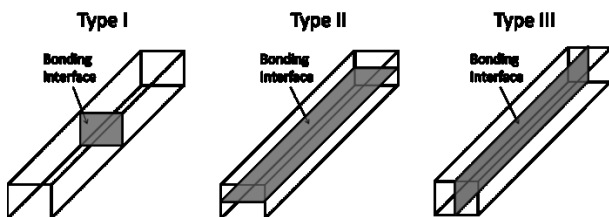


Fig. 3 Illustration of the three configurations of AFB interface orientation investigated in the strength tests.

Analysis of the interferometer images allowed accurate determination of the flexural strain from the clear aperture (A) of the interferograms, the dimensions of the test sample

($w \times t \times L$), the support span (S_s), and the load span (l_s). The maximum deflection (d') within the clear aperture was measured by counting the number of interference fringes within the clear aperture using Zygo MetroPro software. The radius of curvature of the bent surface was calculated as $R = [(A/2)^2 + (d')^2]/(2 \cdot d')$. Subsequently, the total deflection experienced by the sample was calculated as $\Delta = R \cdot [R^2 - (S_s/2)^2]^{1/2}$. The flexural strain was then calculated as:

$$\epsilon_f = \frac{12 \cdot t \cdot \Delta}{S_s^2 \left[3 - \left(1 - \frac{l_s}{S_s} \right)^2 \right]}$$

The flexural stress was estimated from the known load P by the following equation:

$$\sigma_f = \frac{3 \cdot P \cdot (S_s - l_s)}{2 \cdot w \cdot t^2}$$

The Young's modulus was calculated as the ratio between the flexural stress and the flexural strain: $E = \sigma_f / \epsilon_f$.

LIDT testing method

S-on-1 and raster scanning LIDT tests in the nanosecond regime were performed at Lidaris (Vilnius, Lithuania). 1000-on-1 LIDT tests were carried out at ambient conditions following the ISO21254-2 standard using a single-longitudinal-mode 1064 nm Nd:YAG InnoLas SplitLight Hybrid Laser operating at 10.2 ± 0.5 ns pulse duration measured at full width at half maximum (FWHM) and a pulse repetition rate of 100 Hz. The beam at the sample surface showed a Gaussian spatial profile with a $1/e^2$ diameter of 250 ± 5 μm (averaged over 64 pulses). 1000-on-1 LIDT values were retrieved by nonlinear fit to 0% of damage probability and refer to the peak pulse fluence, as defined in the ISO21254-2 standard. Raster scanning tests were carried out to probe the density of defects, which limit large-aperture optics performance. In this study, raster scanning tests were performed to determine whether the presence of a bonding interface affects the probability of laser-induced damage onset. Samples were tested at ambient conditions on a 1 cm^2 square region using the same setup employed for the 1000-on-1 test. All irradiation parameters were kept the same, with the exception of the laser spot $1/e^2$ diameter at the sample surface, which was increased to 970.7 ± 35.5 μm (averaged over 64 pulses). Each site was irradiated with 1000 pulses at a fluence level which was kept constant throughout the raster scanning test. All samples were initially irradiated at a test fluence of 5 J/cm^2 . If no damage was detected over the entire tested area, the raster scanning test was repeated at a fluence of 7.5 J/cm^2 . Test sites were equally spaced by 485 μm and arranged according to a hexagonal geometry distribution, thus achieving a 50% overlap between adjacent sites. Both in the case of the 1000-on-1 and of the raster scanning tests, occurrence and position of damage sites was monitored both during and after each test.

Results and discussion

Characterisation of mechanical properties

Mechanical properties of monolithic and bonded substrates were measured as described in section 2.3. Figure 4 shows interferograms recorded at incrementally increasing loads for one of the bonded samples. The change in fringe density and pattern correlates to the change in surface figure, and therefore to the strain. These interferograms show no evidence of stress concentration at the bonding interface. This shows that the bonding interface does not act a stress concentrator when the substrate is under load.

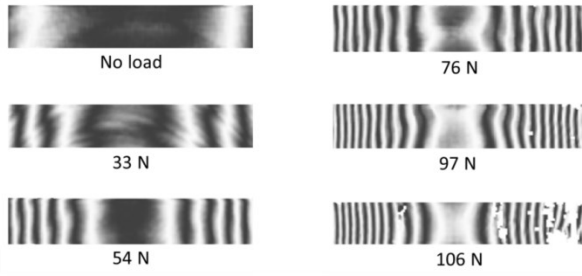


Fig. 4 Interferograms at incrementally increasing load for the Type I bonded sample.

Table 1 summarises the Young's moduli of monolithic and bonded substrates.

Table 1. Young's modulus (E) of monolithic and bonded substrates.

Material configuration	E (GPa)
Monolithic	297 ± 4 GPa
Bonded Type I	295 ± 3 GPa
Bonded Type II	290 ± 2 GPa
Bonded Type III	299 ± 3 GPa

The Young's moduli of all bonded samples are within 3% difference from the Young's modulus of monolithic YAG. The measured value of the Young's modulus of monolithic YAG agrees with values reported in literature [13]. The Young's modulus is a measure of the theoretical cohesive strength of a bulk material, defined as the maximum attractive force between two adjacent atomic layers of a defined orientation as their distance is increased from the equilibrium distance to the onset of fracture. In particular, in the small strain approximation, the theoretical cohesive strength of a bulk material scales as the square root of the Young's modulus [14]. Therefore, results indicate that the bonding interfaces held by London – Van der Waals forces are characterised by a cohesive strength similar to the one characterising atomic layers within a monolithic crystalline sample. Since the Young's moduli of bonded samples do not differ from the Young's modulus of the monolithic substrate and no stress concentration effects were observed in the interferometric measurements, it is reasonable to conclude that the tensile strength of bonded samples is similar to the one of monolithic substrates. While we do not have information about ultimate failure levels, samples were tested to stress values above 120 MPa without sign of fracture onset.

Characterisation of optical properties

Transmitted wavefront measurements were performed over a $22 \text{ mm} \times 22 \text{ mm}$ area (about 92% of the optics aperture) using a Zygo xpD interferometer and analysed using Zygo Mx software. Figure 5(a) shows the wavefront transmitted through a bonded sample after removal of the tilt term. Over the measurement window, the rms wavefront error was 0.01λ and the peak-to-valley wavefront value was 0.085λ for 1030 nm light and for a single pass through the sample. The main contribution to the peak-to-valley value arises from regions of reduced surface quality visible on the right and the bottom sides of the sample. These features originate from the polishing process and are no cause of concern, as they are located outside the operational aperture. The presence of the bonding interface is revealed as a modulation of approximately 0.01λ at the centre of the transmitted wavefront profile. The effect of wavefront distortion on a beam transmitted through the bonded sample was estimated by calculating the point-spread-function (PSF) from the measured wavefront. Figure 5(b) shows the estimated PSF for a square $22 \text{ mm} \times 22 \text{ mm}$ beam, along with an outline up to the second diffraction order. The FWHM

angular spread of the central maximum is $45 \mu\text{rad}$ on both axis and Strehl ratio is 0.997.

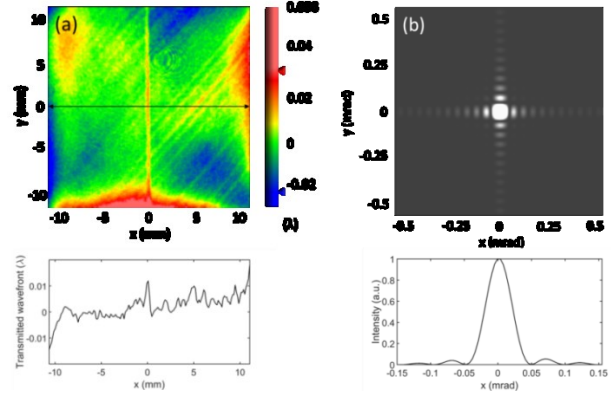


Fig. 5 Transmitted wavefront through a bonded sample and outline (indicated by the black arrow) along x (a). The bonding interface is the vertical line at $x = 0$; the colorscale was modified so to enhance the bonding interface. Beam PSF calculated from the measured transmitted wavefront and its outline up to the second diffraction order along y (b).

The reflected wavefront off both opposite surfaces of a bonded sample was also measured. Due to the parallelism of the faces of the sample, spurious fringes, commonly known as Fizeau fringes, were formed and prevented an accurate measurement of the reflected wavefront. This effect was only partially mitigated by applying a layer of First Contact Polymer™ to the back surface. Figure 6 shows the reflected wavefront for one of the surfaces, along with an outline of the reflected wavefront across the bonding interface. No discontinuity could be observed in the reflected wavefronts, thus indicating that the optical path difference observed in the transmitted wavefront is primarily caused by a refractive index difference at the bonding interface, which, considering $\Delta n = \text{OPD}/d$ and a sample thickness $d = 7 \text{ mm}$, corresponds to $1.5 \cdot 10^{-6}$. Such small difference in refractive index entails low Fresnel reflections at the bonding interface. Ensuring a small refractive index difference is particularly important for amplified spontaneous emission management during high-energy pulse amplification and for maintaining high pulse wavefront quality.

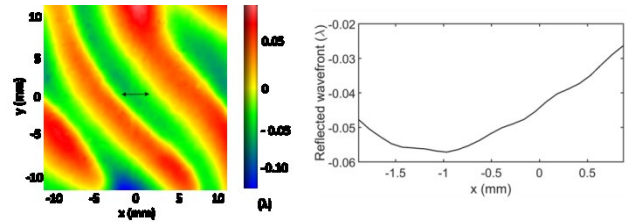


Fig. 6 Reflected wavefront of a bonded sample (a). Outline along x (indicated by the black arrow) around the bonding interface (b).

These measurements confirm that the AFB technology allows meeting the requirements on wavefront aberrations for high-energy laser applications.

LIDT measurements

All samples underwent LIDT testing to characterise their resilience to laser irradiation in the nanosecond regime. Monolithic samples were used to assess the LIDT and defect density of the starting substrate material (in the case of the uncoated sample) and of coated substrates (in the case of the IAD and IBS coated samples). LIDT information on the starting material was used as a reference for evaluating the performance of bonded samples. To this end, both 1000-on-1 and raster scanning LIDT tests were carried out on monolithic samples, using the testing parameters described in section 2.4. Bonded samples underwent raster scanning testing on a square area symmetrically arranged around the bonding region in order to determine if there is an increased damage probability at or near the bonding interface. Results of 1000-on-1 and raster scanning

LIDT tests on monolithic and bonded samples are summarised in Table 2.

Table 2. Front surface 1000-on-1 LIDT and raster scanning damage onset fluence of monolithic and bonded samples, along with the number of observed damage sites over the 1 cm² raster scanned area.

Sample	Front surface 1000-on-1 LIDT (J/cm ²)	Raster scan damage onset fluence (J/cm ²)	Number of damage sites on the raster scanned area
Monolithic uncoated	9.64 ≤ 11.63 ≤ 13.53	5	4
Monolithic IAD coated	9.41 ≤ 10.99 ≤ 12.55	5	6
Monolithic IBS coated	Insufficient data	5	3
Bonded uncoated	-	7.5	3
Bonded IAD coated	-	5	5
Bonded IBS coated	-	5	6

In the case of monolithic samples, the uncoated and the IAD coated substrates showed a LIDT of 11.63 J/cm² and of 10.99 J/cm², respectively. Instead, higher resilience to damage was observed in the case of the IBS-coated sample, for which only 18 sites out of 212 were damaged, with lowest observed damage occurring after 5 pulses at 31 J/cm². The low damage statistics prevented an accurate estimate of the LIDT for this sample. During raster scanning tests, all monolithic samples suffered from sparse damage creation over the 1 cm² scanned area when irradiated at a fluence level of 5 J/cm². Uncoated, IAD coated, and IBS coated monolithic samples exhibited 4, 6 and 3 damage sites, respectively. Both IAD and IBS coated bonded samples showed sparse damage creation over the scanned area when irradiated at a fluence level of 5 J/cm², with 5 and 6 damage sites respectively (Fig. 7(b) and 7(c)). Instead, the uncoated sample did not experience damage onset when irradiated at the same fluence level. In order to induce damage formation on the uncoated sample, the raster scanning test was repeated over the same area at an increased fluence level of 7.5 J/cm² and led to the formation of three damage sites (Fig. 7(a)).

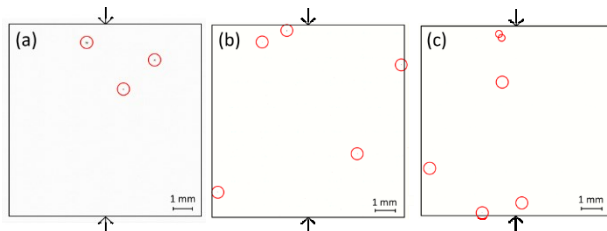


Fig. 7 Microscope images of the raster scanned areas for the uncoated (a), IAD-coated (b), and IBS coated (c) bonded samples. Damage sites are indicated with a circle, the bonding interface is indicated by arrows, and the edge of the raster scanned area is indicated by the solid black square.

As evident from Fig. 7, none of the bonded samples experienced damage formation on or near the bonding interface (indicated by the arrows), thus demonstrating that damage probability in the nanosecond regime was not increased by the presence of a bonding interface.

Conclusions

In this annual report, we presented mechanical and optical characterization of adhesive-free bonded crystalline Yb:YAG substrates. We demonstrated that the mechanical strength of bonded samples is comparable to the mechanical strength of monolithic substrates. Interferometric measurements showed that AFB Yb:YAG meets the wavefront quality requirements for high-energy laser systems. Moreover, LIDT test in the nanosecond regime carried out on both uncoated and coated samples showed that the presence of a bonding interface did not increase the probability of laser-induced damage onset. These results indicate that the AFB technique constitutes a viable alternative for producing large aperture gain media slabs required for high-energy laser systems. Such bonding capability could enable the production of geometries which are not easily obtained via standard growing methods, including structures for the suppression of parasitic oscillations or slabs of graded

dopant concentration. Based on the positive results obtained from the characterization of optical and mechanical properties at room temperature, further experiments, including LIDT testing and laser amplification at cryogenic temperatures, are planned for the near future.

References

1. S. P. D. Mangles, C. D. Murphy, Z. Najmudin, A. G. R. Thomas, J. L. Collier, A. E. Dangor, E. J. Divall, P. S. Foster, J. G. Gallacher, C. J. Hooker, D. A. Jaroszynski, A. J. Langley, W. B. Mori, P. A. Norreys, F. S. Tsung, R. Viskup, B. R. Walton, and K. Krushelnick, "Monoenergetic beams of relativistic electrons from intense laser-plasma interactions," *Nature* **431**, 535-538 (2004).
2. H. Schwoerer, S. Pfotenhauer, O. Jäckel, K. Amthor, B. Liesfeld, W. Ziegler, R. Sauerbrey, K. W. D. Ledingham, and T. Esirkepov, "Laser-plasma acceleration of quasi-monoenergetic protons from microstructured targets," *Nature* **439**, 445-448 (2006).
3. S. Kneip, S. R. Nagel, C. Bellei, N. Bourgeois, A. E. Dangor, A. Gopal, R. Heathcote, S. P. D. Mangles, J. R. Marques, A. Maksimchuk, P. M. Nilson, K. Ta Phuoc, S. Reed, M. Tzoufras, F. S. Tsung, L. Willingale, W. B. Mori, A. Rousse, K. Krushelnick, and Z. Najmudin, "Observation of synchrotron radiation from electrons accelerated in a petawatt-laser-generated plasma cavity," *Phys. Rev. Lett.* **100**, 105006 (2008).
4. M. Dunne, "A high-power laser fusion facility for Europe," *Nat. Phys.* **2**, 2-5 (2006).
5. G. Miller, E. Moses, and C. Wuest, "The national ignition facility," *Opt. Eng.* **43**, 2841-2853 (2004).
6. P. D. Mason, M. Fitton, A. Lintern, S. Banerjee, K. Ertel, T. Davenne, J. Hill, S. P. Blake, P. J. Phillips, T. J. Butcher, J. M. Smith, M. De Vido, R. J. S. Greenhalgh, C. Hernandez-Gomez, and J. L. Collier, "Scalable design for a high energy cryogenic gas cooled diode pumped laser amplifier," *Applied Optics* **54**(13), 4227-4238 (2015).
7. S. Banerjee, K. Ertel, P. D. Mason, P. J. Phillips, M. De Vido, J. M. Smith, T. J. Butcher, C. Hernandez Gomez, R. J. S. Greenhalgh, and J. L. Collier, "DiPOLE: a 10 J, 10 Hz cryogenic gas cooled multi-slab nanosecond Yb: YAG laser," *Optics Express* **23**, 15 19542-51 (2015).
8. S. Banerjee, P. D. Mason, K. Ertel, P. J. Phillips, M. De Vido, O. Chekhlov, M. Divoky, J. Pilar, J. M. Smith, T. J. Butcher, A. Lintern, S. Tomlinson, W. Shaikh, C. Hooker, A. Lucianetti, C. Hernandez-Gomez, T. Mocek, C. Edwards, and J. L. Collier, "100 J-level nanosecond pulsed diode pumped solid state laser," *Optics Letters* **41**, 9 2089-92 (2016).
9. H. E. Meissner, and O. R. Meissner, "Solid state lasers with composite crystal or glass components" U.S. Patent No. 5,852,622. 22 Dec. 1998.
10. H. Lee, H. E. Meissner, and O. R. Meissner, "Adhesive-free bonded (AFB) CVD diamond/sapphire and CVD diamond/YAG crystal composites," *Defense and Security Symposium. International Society for Optics and Photonics* (2006).
11. H. C. Lee and H. E. Meissner, "Characterisation of AFB sapphire single crystal composites for infrared window application," *Proc. of SPIE*, 6545, 65450K-1, (2007).
12. ASTM Standard C1161-02c, "Standard test method for flexural strength of advanced ceramics at ambient temperature".
13. W. Koechner, *Solid-State Laser Engineering* (Springer, 2010).
14. E. Orowan, "Fracture and strength of solids," *Reports on progress in physics* **12.1**, 185 (1949).